



ELSEVIER

Atmospheric Research 72 (2004) 89–105

ATMOSPHERIC
RESEARCH

www.elsevier.com/locate/atmos

First retrieval of cloud phase from SCIAMACHY spectra around 1.6 μm

J.R. Acarreta*, P. Stammes, W.H. Knap

*Atmospheric Research Division, Climate Research and Seismology Department,
Royal Netherlands Meteorological Institute (KNMI, KS-AO), P.O. Box 201,
3730 AE, De Bilt, The Netherlands*

Received 31 July 2003; received in revised form 15 January 2004; accepted 31 March 2004

Abstract

An index for fast thermodynamic cloud phase retrievals, the cloud phase index (CPI), is presented. The index is calculated by fitting the spectral slope of the reflectance around 1.6 μm . It is normalized with the reflectance at 1.64 μm in order to make the index insensitive to calibration constants. A selected set of observations by the Scanning Imaging Absorption Spectrometer for Atmospheric Chartography (SCIAMACHY), an instrument on board the ENVISAT platform, is used. Preliminary results are encouraging, showing a positive index between ≈ 25 and 50 for ice clouds.

© 2004 Elsevier B.V. All rights reserved.

Keywords: Clouds; Thermodynamic properties; Remote sensing; Earth sciences

1. Introduction

Currently, clouds are one of the most interesting elements in the Earth's atmosphere. Indeed, the thermodynamic phase is extremely important for the effects on radiation budget, hydrology or dynamics. Moreover, ice clouds have challenging microphysical properties in terms of shape and size distribution of the irregular ice crystals (Mishchenko et al., 1996; Baum et al., 2000a; Heymsfield et al., 2002). Hence, a

* Corresponding author. Tel.: +31-30-2206-725; fax: +31-30-2210-407.

E-mail address: acarreta@knmi.nl (J.R. Acarreta).

URL: <http://www.knmi.nl/onderzk/index.html>.

procedure to determine the phase of the clouds is needed before any microphysical model can be applied.

The determination of the cloud thermodynamic phase relies on two main techniques. Either reflected solar radiation is considered (Hansen and Pollack, 1970; Baum et al., 2000b) or infrared emission is used (Ou et al., 1993; Baran et al., 2003). Both belong to the passive techniques that combine multispectral information. New missions (ICESAT, CLOUDSAT, CALIPSO or EARTH-CARE) present an improvement over the previous techniques by adding active sensors to satellites (for details about active methods, see Donovan and van Lammeren, 2002; Wang and Sassen, 2002).

The aim of this work is to present an application, using Scanning Imaging Absorption Spectrometer for Atmospheric Chartography (SCIAMACHY) data, of the spectral shape parameter defined by Knap et al. (2002). It is based on the calculation of the slope of the 1.6- μm reflectance spectrum. Several multispectral methods, as the algorithms for MODIS (see, for example, Rolland et al., 2000), rely on the information given by several channels like 0.65, 1.38, 1.6, or 11 μm . However, the work of Knap et al. (2002) considers only the two-point local slope of the reflectance at 1.67 μm . The physical principle for using this approach is related to the different behaviour of the refractive index for liquid water and ice (Fig. 1).

The region around 1.6 μm (Fig. 1) is characterized by a greater absorption due to ice with respect to liquid water. More important is the different spectral slope, which is zero at

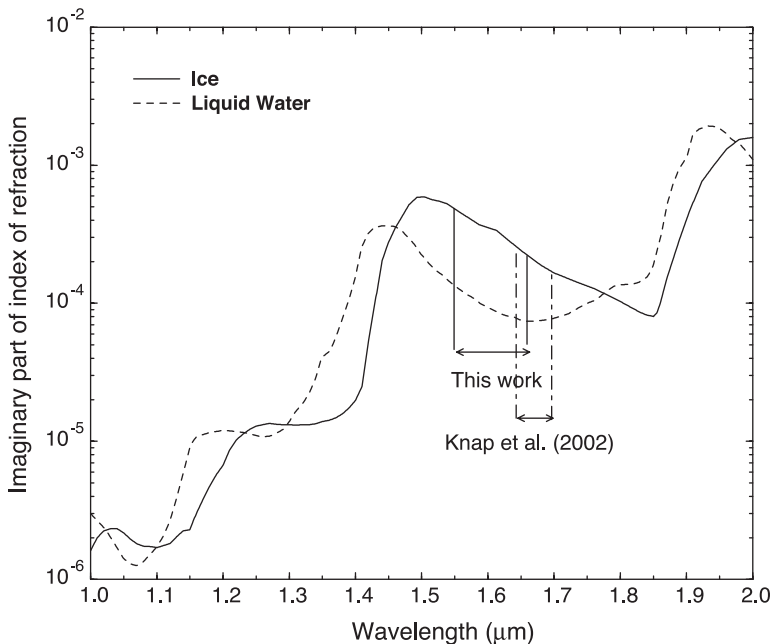


Fig. 1. Imaginary part of the refractive index for liquid water and ice from Downing and Williams (1975) and Warren (1984) (see also Gosse et al., 1995). We show with an arrow the spectral region considered in this work (SCIAMACHY cluster 43) and in Knap et al. (2002).

$\lambda \approx 1.67 \mu\text{m}$ only for liquid water. There is another region with such a property near $1.4 \mu\text{m}$. However, in the latter region, there is a strong effect from the $1.38\text{-}\mu\text{m}$ water vapour absorption band (Gao et al., 1998). In this respect, the $1.6\text{-}\mu\text{m}$ region, besides the CO_2 bands around 1.57 and $1.60 \mu\text{m}$, is an atmospheric window, which permits to infer the thermodynamic phase of the clouds. Further, this spectral region does not contain thermal radiation (Tsay et al., 1996).

The effect of the imaginary part of the refractive index predicts that an ice cloud reflectance spectrum has a positive slope around $1.6 \mu\text{m}$, whereas a water cloud has a slope close to zero. We present in Fig. 2 an example of radiative transfer calculations performed by Knap et al. (2002). We point out that the result shown in Fig. 2 is sensitive to multiple variables, like the geometry, crystal habit, ground albedo, etc. However, the qualitative behavior remains the same: There is an important difference between the spectral slope of ice and liquid water clouds.

The structure of this paper is as follows. The retrieval method of the cloud phase index (CPI) is described in Section 2. A brief description of the satellite data used in this work is presented in Section 3. The behaviour of the SCIAMACHY cloud phase is discussed in Section 4. Finally, we show our conclusions and future work in Section 5.

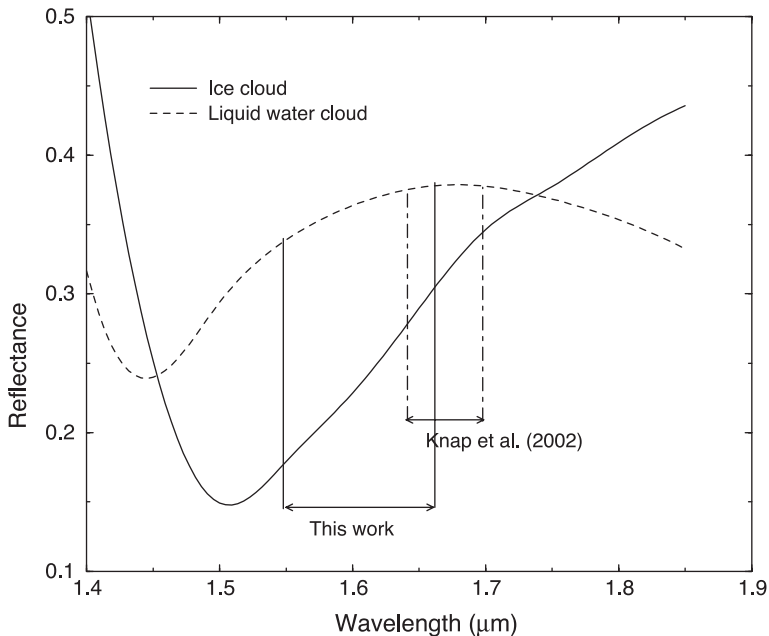


Fig. 2. An example of radiative transfer calculations for a liquid water cloud and an ice cloud. The liquid water cloud contains spherical drops with a size distribution having $10 \mu\text{m}$ effective radius, located between 2 and 3 km in altitude. The ice cloud is composed by columnar imperfect hexagonal ice crystals, with length equal to $60 \mu\text{m}$ and radius equal to $22 \mu\text{m}$. It is located between 8 and 9 km. Both clouds have an optical thickness of 10. More details can be found in Knap et al. (2002).

2. Retrieval method

Our retrieval method consists of defining a CPI. The index is based on a measurement of the spectral slope around 1.6 μm . Using AVIRIS data, [Knap et al. \(2002\)](#) defined the spectral shape parameter $S_{1.67}$ for thermodynamic phase detection as:

$$S_{1.67} = 100 \frac{R_{1.70} - R_{1.64}}{R_{1.64}} \quad (1)$$

where $R_{1.70}$ and $R_{1.64}$ are the measured reflectances at 1.70 and 1.64 μm , respectively. Note that the parameter $S_{1.67}$ is zero for water clouds because of the symmetry of the refractive index of liquid water for wavelengths slightly greater and smaller than 1.67 μm ([Fig. 1](#)). If, as it happens with the data presented in this paper, the spectral interval is not centered around 1.67 μm , the spectral shape parameter is not zero for water clouds.

Due to the technical characteristics of SCIAMACHY (Section 3), the wavelength 1.67 μm is not well suited for a good characterization of the spectral slope, because 1.67 μm is a boundary point in the spectrum where SCIAMACHY changes the spatial resolution. High spatial resolution measurements (60 km across track and 30 km along track), including the 1.6- μm spectral window, are optimal in the spectral region 1.55–1.67 μm . Thus, we choose to reformulate Eq. (1) as follows:

$$\text{CPI} = \frac{6}{R_{1.64}} \times \frac{\partial R}{\partial \lambda} \quad (2)$$

where the derivative is the spectral slope around 1.6 μm with units of reflectance μm^{-1} . In this paper, we calculate the value of the slope as:

$$\frac{\partial R}{\partial \lambda} = \frac{R_{1.67} - R_{1.55}}{1.67 - 1.55} \quad (3)$$

In practice, we find the spectral slope by fitting a straight line to the reflectance spectrum between 1.67 and 1.55 μm . We point out that with this fit, we obtain a more robust value for the slope than by using only two wavelengths. Residual absorption from CO_2 , as well as instrumental artifacts, was removed manually from the fit window (see an example in [Fig. 5](#)). Note that the CPI is insensitive to constant multiplicative calibration factors, due to the factor $R_{1.64}$ in the denominator of Eq. (2).

The comparison of Eqs. (1) and (2) shows that our CPI is similar but not identical to the parameter $S_{1.67}$ of [Knap et al. \(2002\)](#), because of slightly different spectral regions. Therefore, it is expected to find values different from zero for liquid water clouds. Indeed, [Fig. 1](#) shows that our definition will produce slightly positive slopes for water clouds, instead of a zero value. However, for ice clouds, results will be similar. It has been shown with AVIRIS measurements of real cirrus by, among others, [Knap et al. \(2002\)](#) and [Gao et al. \(1998\)](#), that the spectral slope is reasonably constant between 1.55 and 1.70 μm . The calculations of [Fig. 2](#) confirm that our thermodynamic index has slightly positive values for liquid water clouds and that for ice clouds the spectral slope between 1.55 and 1.70 μm is a positive constant.

The CPI for clear pixels is only sensitive to the ground surface, because the atmospheric contribution is negligible. Following [Bowker et al. \(1985\)](#), reflectance curves with zero or

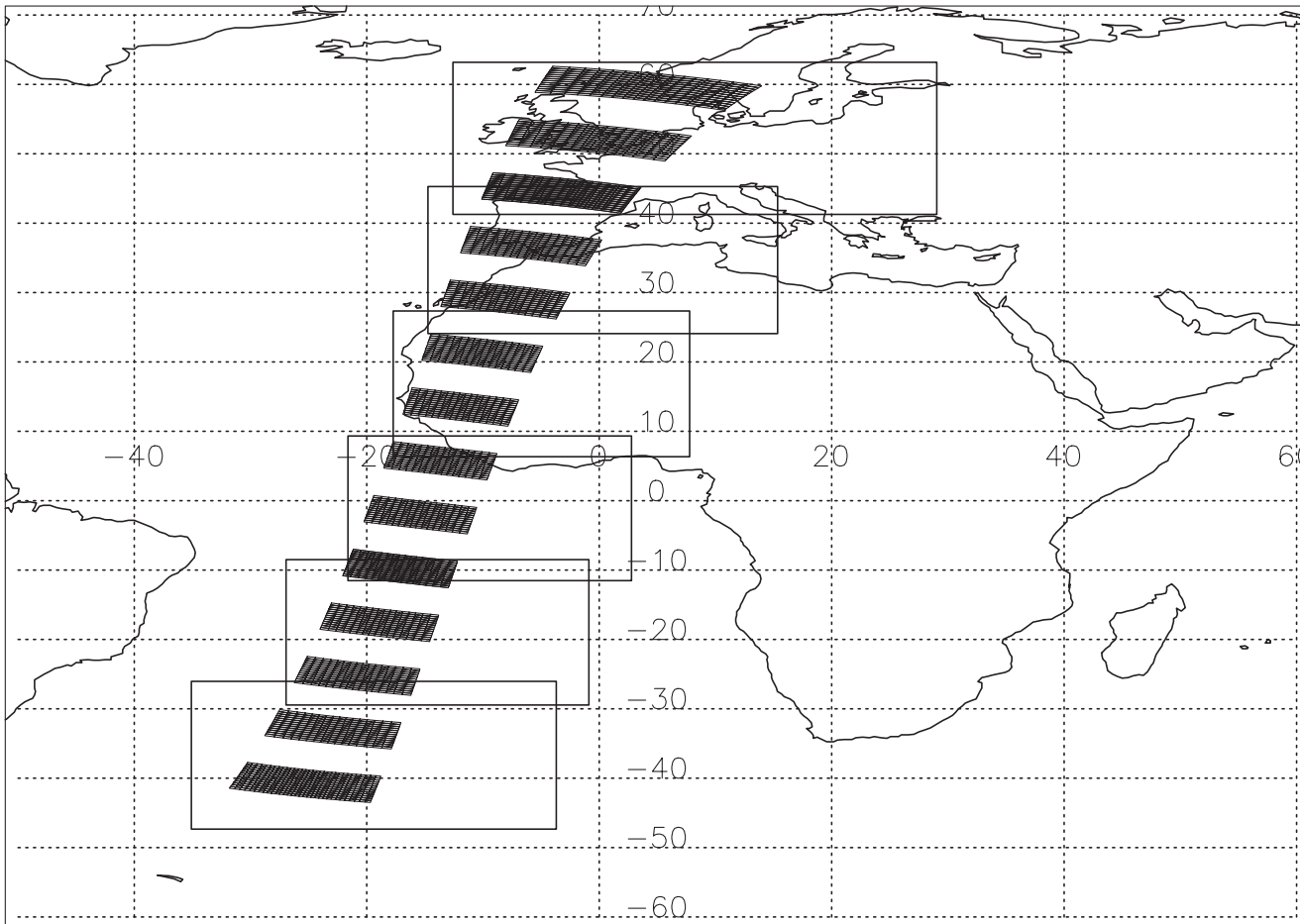


Fig. 3. SCIAMACHY nadir states of the orbit 2510 (black boxes) and MODIS granules (rectangles), both for August 23, 2002.

slightly negative index are due to the ocean, carbonate or quartz beach sands and barley soils. In this work, however, we will use only three types of ground defined as ocean, land and desert (see Section 4).

3. Description of SCIAMACHY and MODIS data

SCIAMACHY is a space-based spectrometer on board the ENVISAT platform, launched in March 2002. A detailed description of the instrument and its performance can be found in Bovensmann et al. (1999). Briefly, it has a spectral range of 0.24–2.38 μm divided in windows named clusters. Each cluster has a different integration time, hence a different spatial resolution. The spectral resolution of SCIAMACHY ranges between 0.24 nm in the UV and 1.56 nm in the NIR.

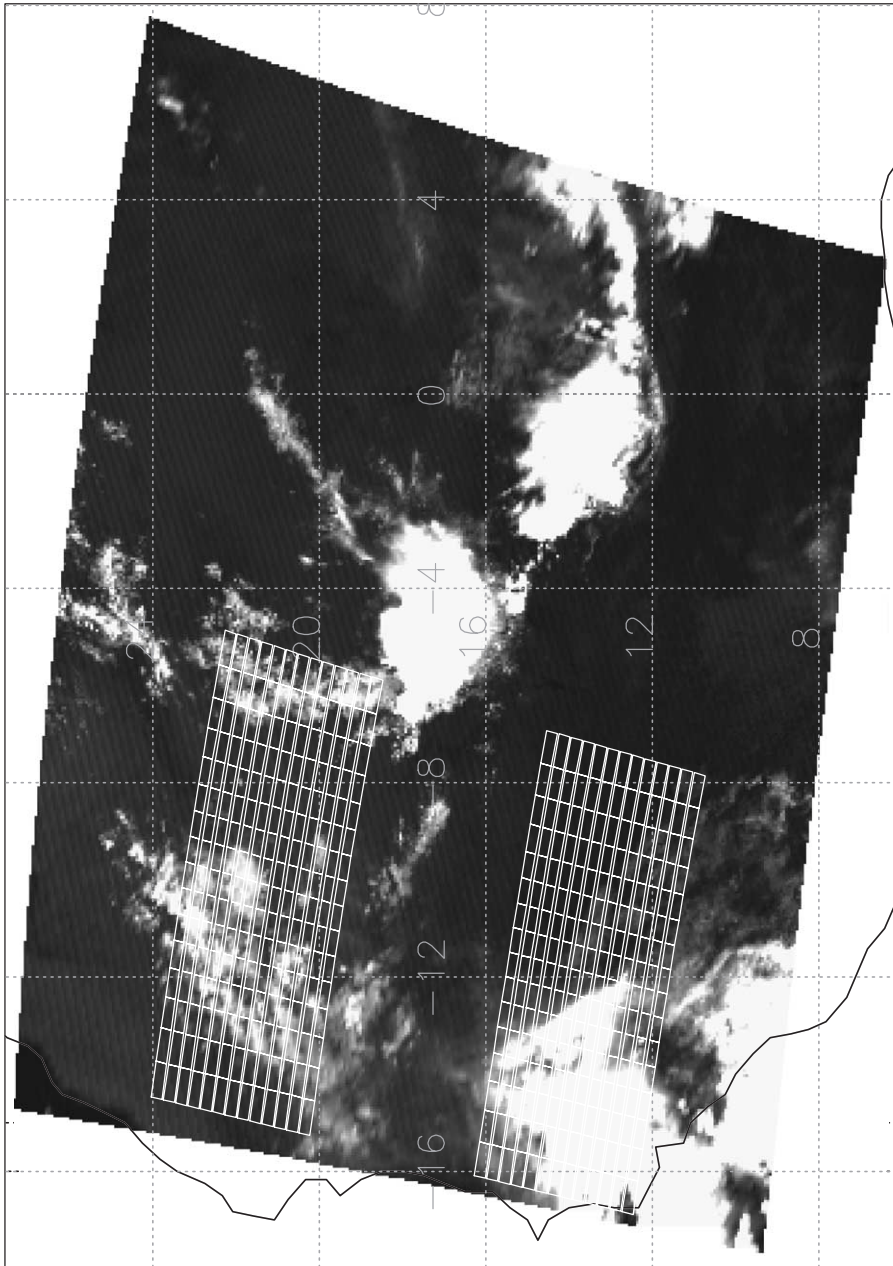
We use in this work cluster 43, between 1.55 and 1.67 μm (see, for instance, Fig. 5), which corresponds to a spatial resolution of $60 \times 30 \text{ km}^2$ (across \times along track) and a spectral resolution of 1.56 nm. This spatial resolution is not kept in the next cluster (number 44), between 1.67 and 1.70 μm ; there the pixel size changes to $240 \times 30 \text{ km}^2$. This, indeed, is the reason for our definition of the slope in the CPI (Eq. 3). One of the features of SCIAMACHY is that the nadir observations are done in a “discontinuous” mode, using regions named states. This feature is due to the limb measurements done by SCIAMACHY between the nadir states. For the orbit considered in this work (number 2510), we show the nadir states as boxes that overlay the ocean and continents (Fig. 3).

We used auxiliary information from the Moderate Resolution Imaging Spectrometer MODIS-TERRA (hereafter MODIS), version 003. Details about the instrumental characteristics of MODIS as well as information related with its products can be found in King et al. (2003) and Platnick et al. (2003). We present in Fig. 4 a comparison of the different spatial resolutions of both instruments. MODIS explores regions (named granules) on the Earth without gaps (the background of Fig. 4), whereas SCIAMACHY samples nadir regions (states), in a non-continuous mode. Fig. 4 also shows small boxes within each SCIAMACHY state that in this work are defined as pixels, i.e., regions of $60 \times 30 \text{ km}^2$.

There is a difference of 0.5 h between the overpass times over the Equator (descending node) of the two sun-synchronous platforms (10:00 for SCIAMACHY and 10:30 for MODIS). It means that the clouds detected by MODIS are not necessarily the same clouds that are seen by SCIAMACHY. To correlate both measurements, when needed, we assumed that the geolocation of MODIS and SCIAMACHY do not have any relative offset and that there is no significant change of the clouds due to the different overpass times. We linearly interpolated the MODIS geolocated products with the SCIAMACHY geolocation grid.

A nice example of the spectral differences between an ice cloud and a liquid water cloud as observed by SCIAMACHY is shown in Fig. 5. The liquid cloud is observed with a viewing zenith angle of 10° and solar zenith angle 31° . The ice cloud is observed with a

Fig. 4. Spatial resolution of SCIAMACHY nadir states for the cluster 43. Each SCIAMACHY state has dimensions of $960 \times 490 \text{ km}^2$. The small boxes are SCIAMACHY pixels, with dimensions $60 \times 30 \text{ km}^2$. The background corresponds to the MODIS Cirrus Reflectance defined by Gao et al. (2002). The grid with geolocation is shown with dashed lines. The thick contour on the left is the northwest coast of Africa (Sahara).



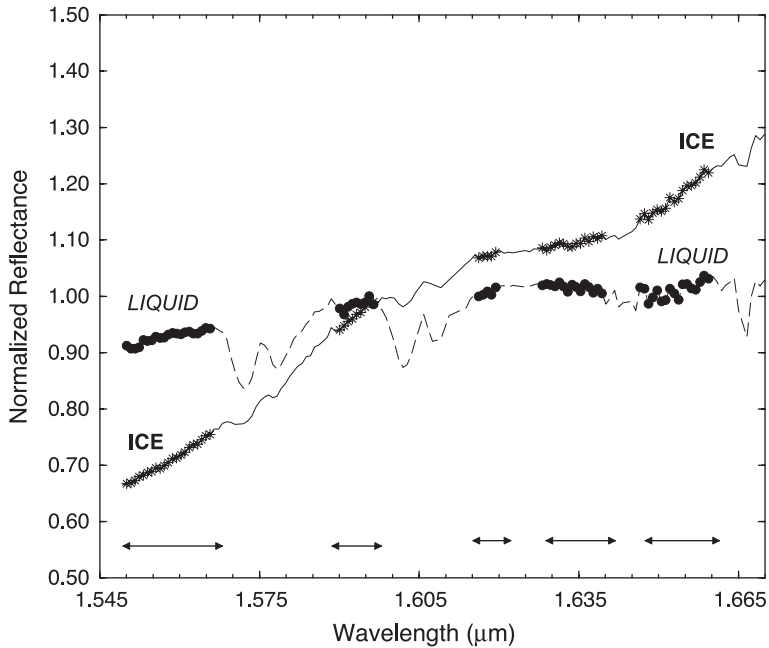


Fig. 5. Example of ice and liquid water cloud spectra measured with SCIAMACHY (cluster 43). Solid and dashed lines are the measurements. Stars and circles show the selected wavelengths included in the spectral fit described in Section 2 (see also the arrows at the bottom). The spectra are normalized by dividing the original data with the mean reflectance of each spectrum.

viewing zenith angle of 22° and a solar zenith angle of 30° . The ground type is the same in both cases (the Sahara desert). Note that both spectra are normalized to one dividing by the mean reflectance. Because the geometry, i.e., the solar and viewing zenith angles, and ground type are similar, the spectral differences in Fig. 5 are solely due to the thermodynamic phase of the clouds.

4. Evaluation of the CPI with MODIS data

In this section, we present an intercomparison of the SCIAMACHY CPI with MODIS data. Our cloud phase index is sensitive to the spectral signature of the ground. Case studies should be defined only over regions with a constant ground type, maximizing as much as possible the number of pixels. Visual analysis of the SCIAMACHY orbit 2510 confirmed that, except for the states over the ocean, there is usually a change in the ground type within each state. Fig. 3 shows that the land type includes regions from the South (Spain) to the North (Finland) of Europe.

We started with the International Geosphere Biosphere Program (IGBP) surface type classification. We found that the surface types of those regions are available on line at the Clouds and the Earth's Radiant Energy System (CERES) web page, within the framework of the Surface and Atmospheric Radiation Budget (SARB) working group (see also Global

Soil Data Task, 2000). Those types, for the selected SCIAMACHY orbit, are forests (evergreen and deciduous, needleleaf and broadleaf) and mosaics of cropland and natural vegetation. However, for the purpose and scope of this paper, we found that the IGBP classification was too detailed.

In consequence, a more simple classification has been introduced in terms of three categories defined by us as ocean, land and desert. The categories are based on the value of the albedo A_λ of the surface covered by each SCIAMACHY pixel. Using as a reference the wavelength $\lambda = 0.75 \mu\text{m}$, we defined the ground types as follows: ocean ($A_{0.75} < 0.08$), land ($0.08 < A_{0.75} < 0.28$) and desert ($0.28 < A_{0.75} < 0.60$). The mapping between each SCIAMACHY pixel and the ground type (ocean, land, desert) is based on the surface albedo database of Koelmeijer et al. (2003) available for different wavelengths. Hence, given the central latitude (φ) and longitude (l) of each SCIAMACHY pixel, it is possible to look up the ground albedo database $A_{0.75}(\varphi, l)$. Once the ground albedo is known, we classify the pixel as ocean, land or desert. We plotted each of our categories on a map to verify that, for instance, all the pixels flagged as ocean are indeed over the ocean.

The CPI data for each of the three ground types was analyzed with two data filters (thresholds) based on the MODIS data. The first filter is the MODIS Cloud Optical Thickness. It is used to decide if a pixel is cloudy or not. We use $\tau_{\text{MODIS}} < 0.1$ for cloud free pixels. That is a conservative threshold, because $\tau_{\text{MODIS}} \approx 0.2$ represents the transition between clear and cloudy pixels for MODIS (Dessler and Yang, 2003). As was stated previously, the MODIS value is an interpolated value using the geolocation of SCIAMACHY. The process takes into account the four corners of each SCIAMACHY pixel, taking the mean value of the four MODIS interpolated values. Interestingly, we found that our histograms are almost identical when we use as a MODIS value the average of all the MODIS pixels (5-km resolution) within each SCIAMACHY pixel.

The second filter is based on the MODIS Cirrus Reflectance product of Gao et al. (2002). That product holds for the region $0.4\text{--}1.0 \mu\text{m}$ (B.C. Gao, personal communication). The simulations performed by Nasiri et al. (2002) in their work for the cirrus models for MODIS showed that the reflectance at $0.65 \mu\text{m}$ (representative of the optical region) is highly sensitive to the ice cloud optical thickness (for values $0\text{--}20$), but it is not a strong function of either the size or habit distribution. Thus, the use of the Cirrus Reflectance is equivalent to the use of the (ice) cloud optical thickness as a threshold. We use in this work a moderate lower threshold of 0.20 for the Cirrus Reflectance, which is equivalent to an ice optical thickness of about 3, following, among others, Baum et al. (2000a), Ou et al. (1993) or Nasiri et al. (2002).

We recall that MODIS has a cloud phase product with the purpose of flagging a pixel as ice, liquid water or mixed phase. With the limited set of data available for this work, the use of the Cirrus Reflectance product is more suitable, because it is a continuous variable (i.e., not a mask like the cloud phase). Therefore, it gives us the opportunity of selecting optically thin or thick cirrus. However, future work might include the MODIS cloud phase as well.

4.1. Retrievals over ocean, land and desert

We show in Fig. 6 the histograms of CPI for the different ground types. The histograms are made with 10 bins, with lower and upper limits equal to -5 and 60 , respectively. The

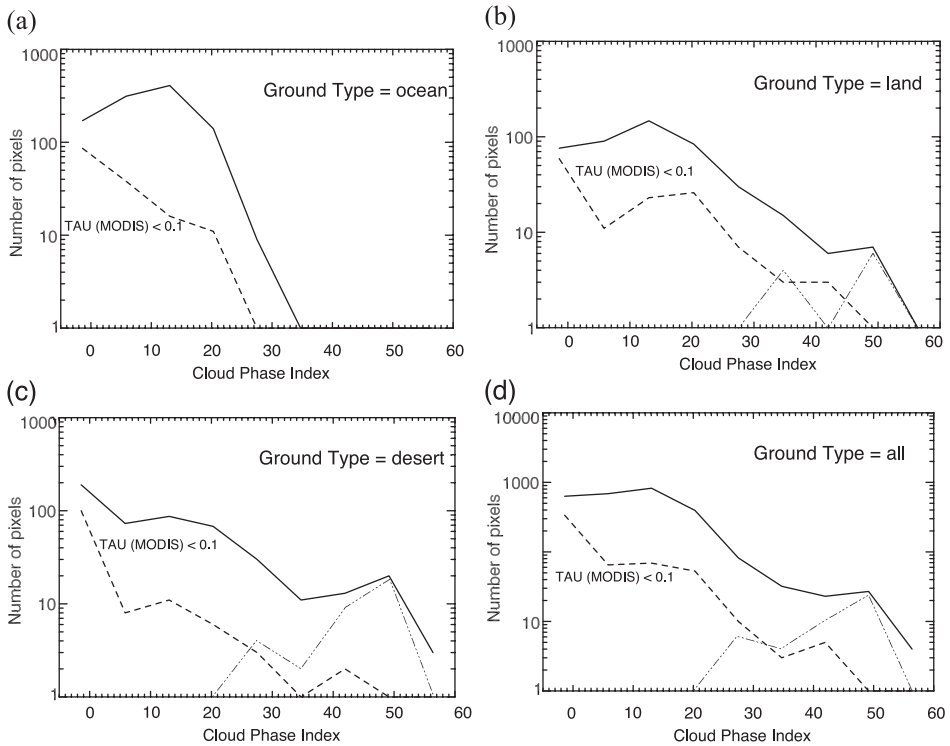


Fig. 6. The solid lines show the histogram of the SCIAMACHY CPI values for the pixels over (from top to bottom) ocean (a), land (b) and desert (c). The dashed line shows the result of adding the threshold $\tau_{MODIS} < 0.1$. The dash–dot line includes the threshold MODIS Cirrus Reflectance > 0.2 . The label in the upper right part of each plot shows the ground type. The label “all” (plot labeled as d) includes all the SCIAMACHY pixels over ocean, land and desert.

vertical axis shows the number of pixels per bin in a logarithmic scale. Fig. 6 contains also the different thresholds based on MODIS data. We point out that the aim is to show a qualitative picture of the meaning of the CPI in different situations.

The main conclusion of Fig. 6 is that when clear pixels are selected ($\tau_{MODIS} < 0.1$), the CPI values move towards zero. However, when pixels with ice clouds are selected, they move in the opposite direction. It is clear that the region $CPI > 20–25$ represents the place where ice clouds can be found, as it is shown by the curves with Cirrus Reflectance greater than 0.2. It is interesting to recall that we are not selecting pixels with a special geometry. Even with such a combination of geometries, it is possible to clearly see different families of curves. Within each curve, we see different peaks. We caution that we use a logarithmic scale for the number of pixels. Thus, not all the peaks are equally significant.

As a first approximation, we can define two representative values for the CPI. One of them is $CPI \approx 10–15$ and the other one $CPI \approx 40–50$. There might be added a third one, $CPI \approx 0$. Interestingly, the peak at $CPI \approx 0$ for clear pixels is more apparent with the surface types desert and ocean than land. The land type contains mainly vegetated scenes but with different types of soils. This might explain the difference. Pixels flagged as ocean

show a well-defined peak around $\text{CPI} \approx 10\text{--}15$, a value that also appears as a peak with the other ground types. We did not find ice clouds with a MODIS Cirrus Reflectance greater than 0.2 over the ocean.

To verify the possibility of detecting liquid water clouds around $\text{CPI} \approx 10\text{--}15$, we present SCIAMACHY observations and simulations of the reflectances $R(1.6)$ and $R(0.5)$ for the pixels over the ocean (Fig. 7). The points of Fig. 7 have a mean CPI of 10 and a standard deviation (1σ) equal to 7. The points with $\text{CPI} \approx 0$ are located at $R(1.6) \approx 0$ and $R(0.5) \approx 0.1$. We used the radiative transfer code Doubling Adding KNMI (DAK) (Stammes, 2001; De Haan et al., 1987). In these calculations, we assumed an atmosphere with clouds but no aerosols, over an ocean simulated with a Lambertian reflector with fixed albedo. We assumed that the clouds, approximated as plane parallel scattering layers, cover homogeneously the scene. The clouds have a log normal distribution of drops with mean effective radius of $10\ \mu\text{m}$ and effective variance 0.1. The cloud is situated between 1 and 2 km in altitude. Simulations are performed for values of the cloud optical thickness equal to 0, 10, 20 and 30. The Lambertian surface albedo for the ocean is set equal to 0.06 at $0.5\ \mu\text{m}$ and 0.02 at $1.6\ \mu\text{m}$ (Sun-Mack et al., 1999). The variations in the simulated reflectance due to the differences in geometry of each pixel are shown as error bars.

In general, the agreement in Fig. 7 is good. However, we find relative offsets around 0.02–0.04 reflectance units in the model simulations with respect to the SCIAMACHY

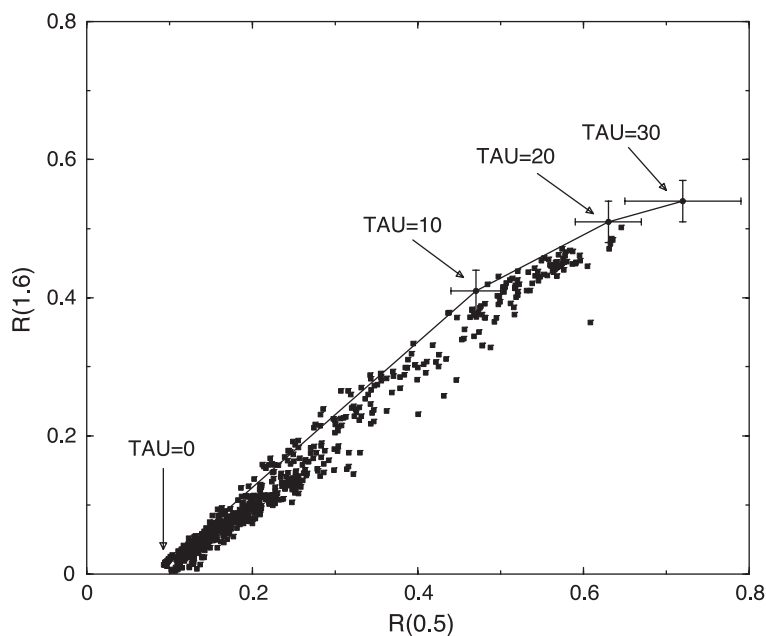


Fig. 7. Reflectance at $1.6\ \mu\text{m}$ versus reflectance at $0.5\ \mu\text{m}$ measured by SCIAMACHY for all pixels over ocean. These points have a mean CPI of 10 and correspond to pixels with liquid water clouds. The solid line represents simulations for different values of the cloud optical thickness. The error bars in the simulations are the expected variations due to geometrical effects.

observations at 0.5 μm . This effect might be a calibration offset. It might be due also to an improper characterization of the water clouds in our simulations; larger particles have more absorption, decreasing $R(1.6)$ in Fig. 7. Nevertheless, it is very reasonable to conclude that clouds with CPI around 10 are liquid water clouds.

A remarkable result is the histogram (see Fig. 6d) with all (2700) SCIAMACHY pixels. Note that it contains all the pixels over the three types of ground (ocean, land, desert) with different viewing geometries. In spite of that, the MODIS thresholds show two important facts. The first one is the accumulation of clear pixels and pixels with liquid water clouds for low values of the CPI. The second one is the detection of ice clouds for high values of the CPI. Note that within the ice cloud category (high value of CPI) a distribution of particle size, crystal habit or optical thickness is expected. Moreover, scenes with multiple cloud layers are also expected. Nevertheless, two distinct peaks are visible for liquid water and ice clouds.

We present in Fig. 8 a plot with the observed SCIAMACHY reflectances $R(0.5)$ and $R(1.6)$ for all the pixels (over ocean, land and desert), binning with the CPI value and, at the same time, including the lower threshold of 0.2 for the MODIS Cirrus Reflectance. Basically, $R(0.5)$ is sensitive to the cloud optical cloud thickness, whereas $R(1.6)$ gives information about the particle size. There are different branches that do not cover the same ranges in $R(0.5)$ and $R(1.6)$. High (≈ 40 – 50) CPI values show a horizontal branch with a narrow range of values for $R(1.6)$, a fact that can be related to a higher sensitivity of the CPI to the crystal size than to the optical thickness. This is

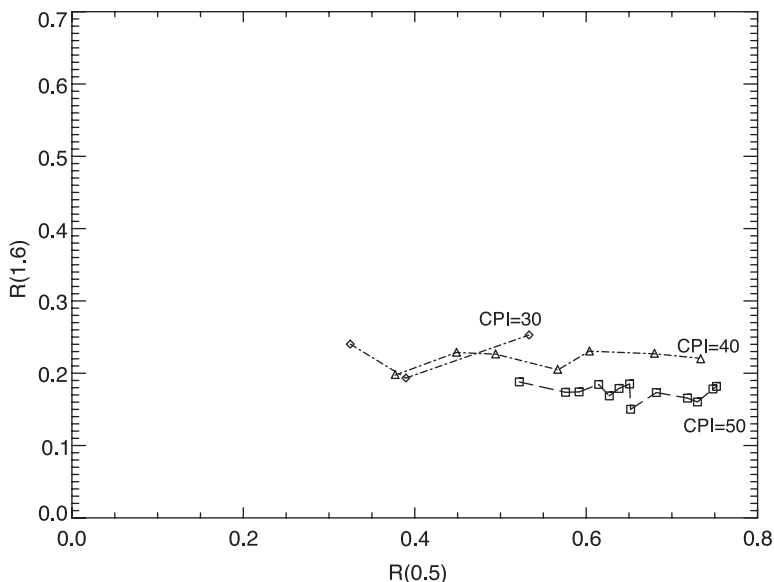


Fig. 8. Reflectance at 1.6 μm versus reflectance at 0.5 μm measured by SCIAMACHY for all pixels over ocean, land and desert for which the MODIS Cirrus Reflectance is greater than 0.2. The different symbols correspond to different values of the CPI index. The different lines connecting data points with the same CPI are included for readability of the figure. The plot only contains pixels with ice clouds.

in agreement with simulations for ice clouds done by others (see Baum et al., 2000b; Knap et al., 2002; Nasiri et al., 2002; Ou et al., 1999; Rolland et al., 2000).

4.2. Sensitivity of CPI to geometry

We explored the sensitivity of the CPI to the geometry with radiative transfer calculations. Ice crystals were considered as randomly oriented columns with certain degree of roughness (Hess et al., 1998). We used two sizes: crystals which have a length of 60 μm and radius of 22 μm (hereafter small) and crystals with dimensions of 130 and 40 μm , respectively (hereafter big). The ground albedo was fixed to 0.02 ($\lambda = 1.6 \mu\text{m}$) in order to be equivalent to the ocean. The viewing zenith angle was fixed to 15° (which is considered representative for all SCIAMACHY pixels). The solar zenith angle was varied between 0° and 75° (six equally spaced angles) and the relative azimuth angle was considered equal to 0° , 45° , 90° , 135° and 180° . We included four values of the ice optical thickness equal to $\tau_{\text{ICE}} = 1, 3, 5$ and 7 . The results are shown in Fig. 9 for azimuth 0° only. Clearly, the solar zenith angle dependence of the CPI is small. Because of symmetry, we expect that also the viewing zenith angle dependence of the CPI is small. Indeed, this was confirmed by CPI calculations at other viewing angles.

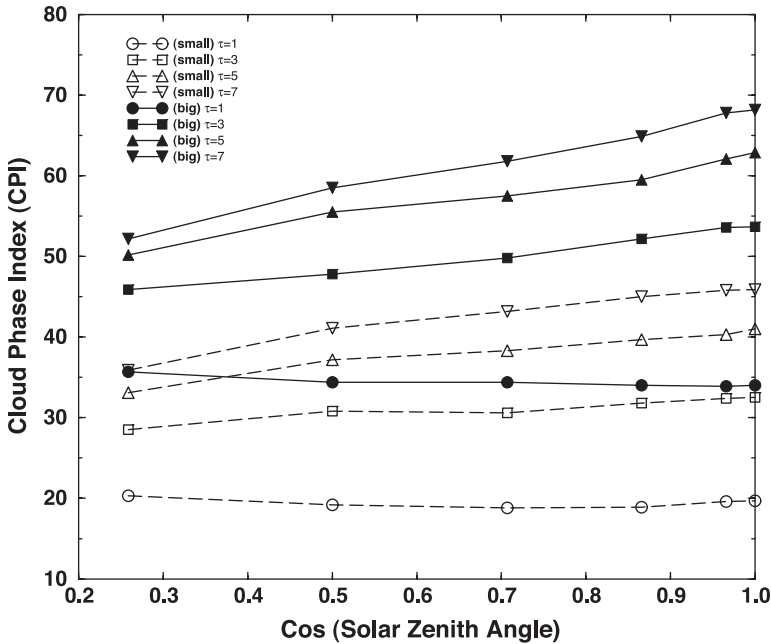


Fig. 9. Simulations of the CPI as a function of the solar zenith angle, for a relative azimuth of 0° and a viewing zenith angle of 15° . Other geometries show a similar behavior. The meaning of “big” and “small” ice particles is described in Section 4.2. The symbols circle, square, triangle up and triangle down indicate the ice optical thickness. Big ice particles are shown with solid lines and black symbols. Small ice particles are shown with dashed lines and white symbols.

We found (Fig. 9) that for the smallest crystal size, values of ice optical thickness up to 7 produce CPI values less or similar to ≈ 40 . However, for the largest crystals, an ice optical thickness of ≈ 3 –5 gives values around 50. We point out that with our set of observations the mode of Fig. 6 is around CPI ≈ 50 for thick cirrus clouds. As was stated previously, the MODIS cirrus reflectance threshold considered in this work is equivalent to an ice optical thickness greater or equal than 3. Thus, our conclusion is that if we assume thick cirrus the large particles reproduce much better the range of CPI values for thick cirrus than the smaller particles.

We calculated the mean and standard deviation of the CPI for all the geometries (note that Fig. 9 shows only one geometry) and for each value of the ice optical thickness. We found that, for the big particles, the CPI value for our selected MODIS cirrus reflectance threshold (equivalent to $\tau_{\text{ICE}}=3$) is 49.8 ± 0.5 . Values for the ice optical thickness smaller and greater than 3 give CPI values equal to 31.4 ± 0.8 ($\tau_{\text{ICE}}=1$) and 58.3 ± 0.6 ($\tau_{\text{ICE}}=5$). Note the small spread (a few percent) due to varying geometry. Higher values for the ice optical thickness ($\tau_{\text{ICE}}=7$) give too high CPI values ≈ 63 . Note how the CPI derived from the observations (≈ 50) is indeed included in the interval defined by the values $\tau_{\text{ICE}}=1$ and $\tau_{\text{ICE}}=5$. On the other hand, due to the incompatibility with the observations, we do not present the sensitivity for the small particles. In any case, the example of Fig. 9 shows that there is not significant change in the CPI sensitivity between small and big particles.

In conclusion, we find that, first, the sensitivity of our cloud phase index to the geometry is small. Second, for this limited set of observations, the CPI values are compatible with a crystal size around $130 \mu\text{m}$ (big particles). We caution that our finding is only representative under the assumption that the crystal shape is reasonable correct, and that the number of SCIAMACHY pixels with cirrus that was studied is small. Future work is needed to show if our model holds in all circumstances.

5. Conclusions and outlook

In this work, we have presented a new index, called CPI, for the determination of the cloud thermodynamic phase. The index has been applied to a limited set of observations by SCIAMACHY, on board the ENVISAT platform. MODIS products are used to preliminarily intercompare the properties of the CPI.

The limited set of SCIAMACHY observations available at this moment makes it difficult to apply radiative transfer calculations of ice clouds exploring all the sensitivities and values for the free parameters. However, several radiative transfer calculations show agreement with our SCIAMACHY findings for both liquid and ice clouds. It has been found that the sensitivity of the CPI to the geometry is small. It has been shown that the SCIAMACHY cloud phase index is highly correlated with the MODIS cloud optical thickness and the cirrus reflectance. CPI values around 0 can be found for cloud-free pixels. We have found that the CPI is positive with values less than 50, which is compatible with the results of Knapp et al. (2002). Water clouds have a CPI around 10. Thick ice clouds (optical thickness greater than 3) have $\text{CPI} > 20$ –25.

The cloud phase index defined in this work is somewhat sensitive to the slope of the spectral reflectance of the ground, but not to the exact value of the ground albedo. As a result, future work could study the sensitivity of the CPI to well-defined ground types. A starting point could be radiative transfer calculations coupled with the surface reflectance curves of Bowker et al. (1985). It would be interesting to quantify with more data how sensitive the CPI is to the horizontal inhomogeneity of cirrus clouds. Note that shadow effects might be important as well. However, for the large pixel size of SCIAMACHY ($30 \times 60 \text{ km}^2$), those effects are considered to be second order effects.

In the future, much more state-of-the-art calibrated SCIAMACHY data will be available. It will be possible, for instance, to chart the different cirrus types (e.g., Sassen and Comstock, 2001) with the CPI index. At the same time, it will be possible to use detailed radiative transfer calculations for ice crystals to provide us with a better microphysical interpretation of the cloud phase index. A proper validation will be achieved after a direct comparison with in situ measurements from, for instance, SIRTa (France), ARM (USA) or Cabauw (The Netherlands) is done. The use of MERIS (also on board ENVISAT) high-resolution images could improve our clear/cloudy mask, because the clouds seen by MERIS and SCIAMACHY are the same in terms of temporal and spatial geolocation. It is interesting to mention that in such a validation, it might be possible to include more spectral information available from SCIAMACHY, such as the reflectance at $0.477 \mu\text{m}$ ($\text{O}_2\text{-O}_2$ absorption band), $0.76 \mu\text{m}$ ($\text{O}_2\text{-A}$ absorption band) or $1.38 \mu\text{m}$ (H_2O absorption band).

Acknowledgements

This work has been funded by Space Research Organization of the Netherlands (SRON), under project SCIA-CIRRUS (EO-047). We thank L.G. Tilstra (KNMI) for many valuable discussions about the instrumental features of the SCIAMACHY data. The European Space Agency (ESA) is acknowledged as the source of the SCIAMACHY data. The European Space Agency (ESA) is acknowledged as the source of the SCIAMACHY data. The data used in this study were acquired as part of the NASA's Earth Science Enterprise. The algorithms were developed by the MODIS Science Teams. The data were processed by the MODIS Adaptive Processing System (MODAPS) and Goddard Distributed Active Archive Center (DAAC), and are archived and distributed by the Goddard DAAC. We thank the two anonymous reviewers for their helpful comments on the manuscript.

References

- Baran, A.J., Francis, P.N., Yang, P., 2003. A process study of the dependence of ice crystal absorption on particle geometry: application to aircraft radiometric measurements of cirrus cloud in the terrestrial window region. *J. Atmos. Sci.* 60, 417–427.
- Baum, B.A., Kratz, D.P., Yang, P., Ou, S.C., Hu, Y., Soulen, P.F., Tsay, S.C., 2000a. Remote sensing of cloud properties using MODIS airborne simulator imagery during SUCCESS: 1. Data and models. *J. Geophys. Res.* 105, 11767–11780.

- Baum, B.A., Soulen, P.F., Strabala, K.I., King, M.D., Ackerman, S.A., Menzel, P., Yang, P., 2000b. Remote sensing of cloud properties using MODIS airborne simulator imagery during SUCCESS: 2. Cloud thermodynamic phase. *J. Geophys. Res.* 105, 11781–11792.
- Bovensmann, H., Burrows, J.P., Buchwitz, M., Frerick, J., Noël, S., Rozanov, V.V., Chance, K.V., Goede, A.P.H., 1999. SCIAMACHY: mission objectives and measurement modes. *J. Atmos. Sci.* 56, 127–150.
- Bowker, D.E., Davis, R.E., Myrick, D.L., Stacy, K., Jones, W.T., 1985. Spectral reflectances of natural targets for use in remote sensing studies. NASA Ref. Publ. 1139, 1–181.
- De Haan, J.F., Bosma, P.B., Hovenier, J.W., 1987. The adding method for multiple scattering calculations of polarized light. *Astron. Astrophys.* 183, 371–393.
- Dessler, A.E., Yang, P., 2003. The distribution of tropical thin cirrus clouds inferred from Terra MODIS data. *J. Climate* 16, 1241–1247.
- Donovan, D.P., van Lammeren, A.C.A.P., 2002. First ice cloud effective particle size parametrization based on combined lidar and radar data. *Geophys. Res. Lett.* 29, 1–4.
- Downing, H.D., Williams, D., 1975. Optical constants of water in the infrared. *J. Geophys. Res.* 80, 1656–1661.
- Gao, B.C., Kaufman, Y.J., Han, W., Wiscombe, W.J., 1998. Correction of thin cirrus path radiance in the 0.4–1.0 μm spectral region using the sensitive 1.375 μm cirrus detecting channel. *J. Geophys. Res.* 103, 32169–32176.
- Gao, B.C., Yang, P., Han, W., Li, R.R., Wiscombe, W.J., 2002. An algorithm using visible and 1.38 μm channels to retrieve cirrus cloud reflectances from aircraft and satellite data. *IEEE Trans. Geosci. Remote Sens.* 40, 1659–1667.
- Global Soil Data Task, 2000. Global Soil Data Products CD-ROM (IGBP-DIS). CD-ROM. International Geosphere Biosphere Programme. Data and Information System, Postdam, Germany. Available from Oak Ridge National Laboratory Distributed Active Archive Center, Oak Ridge, Tennessee, USA (web page of the Oak Ridge National Laboratory).
- Gosse, S., Labrie, D., Chylek, P., 1995. Refractive index of ice in the 1.4–7.8 μm spectral range. *Appl. Opt.* 34, 6582–6586.
- Hansen, J.E., Pollack, J.B., 1970. Near infrared scattering by terrestrial clouds. *J. Atmos. Sci.* 27, 265–281.
- Hess, M., Koелеmeijer, R.B.A., Stammes, P., 1998. Scattering matrices of imperfect hexagonal crystals. *J. Quant. Radiat. Transfer* 60, 301–308.
- Heymsfield, A.J., Bansemir, A., Field, P.R., Durden, S.L., Stith, J.L., Dye, J.E., Hall, W., Grainger, C.A., 2002. Observations and parameterizations of particle size distributions in deep tropical cirrus and stratiform precipitating clouds: results from in situ observations in TRMM field campaigns. *J. Atmos. Sci.* 59, 3457–3491.
- King, M.D., Menzel, W.P., Kaufman, Y.J., Tanré, D., Gao, B.C., Platnick, S., Ackerman, S.A., Remer, L.A., Pincus, R., Hubanks, P.A., 2003. Cloud and aerosol properties, precipitable water, and profiles of temperature and humidity from MODIS. *IEEE Trans. Geosci. Remote Sens.* 41, 442–458.
- Knap, W.H., Stammes, P., Koелеmeijer, R.B.A., 2002. Cloud thermodynamic phase determination from near infrared spectra of reflected sunlight. *J. Atmos. Sci.* 59, 83–96.
- Koелеmeijer, R.B.A., De Haan, J.F., Stammes, P., 2003. A database of spectral surface reflectivity in the range 335–772 nm derived from 5.5 years of GOME observations. *J. Geophys. Res.* 107 (doi: 10.1029/2002JD002429).
- Mishchenko, M.I., Rossow, W.B., Macke, A., Lacis, A.A., 1996. Sensitivity of cirrus cloud albedo, bi-directional reflectance and optical thickness retrieval accuracy to ice particle shape. *J. Geophys. Res.* 101, 16973–16985.
- Nasiri, S.L., Baum, B.A., Heymsfield, A.J., Yang, P., Poellot, M.R., Kratz, D.P., Hu, Y., 2002. *J. Appl. Meteorol.* 41, 197–217.
- Ou, S.C., Liou, K.N., Gooch, W.M., Takano, Y., 1993. Remote sensing of cirrus cloud properties using AVHRR 3.7 and 10.9 μm channels. *Appl. Opt.* 32, 2171–2180.
- Platnick, S., King, M.D., Ackerman, S., Menzel, W.P., Baum, B.A., Riédi, J.C., Frey, R.A., 2003. The MODIS cloud products: algorithms and examples from Terra. *IEEE Trans. Geosci. Remote Sens.* 41, 459–473.
- Rolland, P., Liou, K.N., King, M.D., Tsay, S.C., McFarquhar, G.M., 2000. Remote sensing of optical and microphysical properties of cirrus clouds using moderate resolution imaging spectroradiometer channels: methodology and sensitivity to physical assumptions. *J. Geophys. Res.* 105, 11721–11738.
- Sassen, K., Comstock, J.M., 2001. A midlatitude cirrus cloud climatology from the facility for atmospheric remote sensing: Part III. Radiative properties. *J. Atmos. Sci.* 58, 2113–2127.

- Stammes, P., 2001. Spectral radiance modeling in the UV–visible range. In: Smith, W.L., Timofeyev, Y.M. (Eds.), *IRS2000: Current Problems in Atmospheric Radiation*. A. Deepak Publ., Hampton, VA, pp. 385–388.
- Sun-Mack, S., Chen, Y., Murray, T.D., Minnis, P., Young, D.F., 1999. Visible and clear-sky and near-infrared surface albedos derived from VIRS data for CERES. *Proc. AMS 10th Conf. Atmos. Rad.*, Madison, WI, June 28–July 2, American Meteorological Society, Boston, MA, 422–425.
- Tsay, S.C., Gabriel, P.M., King, M.D., Stephens, G.L., 1996. Spectral reflectance and atmospheric energetics in cirrus like clouds: Part II. Applications of a fourier riccati approach to radiative transfer. *J. Atmos. Sci.* 53, 3450–3467.
- Wang, Z., Sassen, K., 2002. Cirrus cloud microphysical property retrieval using lidar and radar measurements: Part I. Algorithm description and comparison with in situ data. *J. Appl. Meteorol.* 41, 218–229.
- Warren, S.G., 1984. Optical constants of ice from the ultraviolet to the microwave. *Appl. Opt.* 23, 1206–1225.